Journal of Colloid and Interface Science **249,** 104–112 (2002)
doi:10.1006/jcis.2002.8218, available online at http://www.idealibrary.com on IDEAL®

Effect of Mordenite Dealumination on the Structure of Encapsulated Molybdenum Catalysts

Mohamed Mokhtar Mohamed*,[1] and Tarek M. Salama†

*Chemistry Department, Faculty of Science, Benha University, Benha, Egypt; and †Chemistry Department, Faculty of Science, Al-Azhar University, Naser City 11884, Cairo, Egypt

Received June 1, 2001; accepted January 11, 2002; published online March 26, 2002

A series of dealuminated mordenites treated under various conditions of acid leaching was impregnated in an aqueous solution of ammonium heptamolybdate to achieve a loading of 12 wt% Mo. These samples were characterized by XRD, UV-DRS, N_2 adsorption, TGA, and FTIR techniques. Special attention was given to the far-IR measurements and IR study of surface hydroxyl groups before and after dealumination. A polymolybdate species was recognized by the appearance of bands at 344, 319, and 236 (229) cm^{-1} due to the vibrational modes of δ(Mo–O) and δ(Mo–O–Mo), respectively. The disappearance of the 236 cm^{-1} band as well as that at 344 cm^{-1} in favor of the 319 cm^{-1} band, with the dealumination, was related to the high dispersion of Mo species in the produced mesopore surface assessed by the N_2 adsorption at 77 K. No bands due to bulk MoO_3 were detected from the IR and XRD results. A strong interaction between Mo species and dealuminated mordenite surfaces (OH groups) was recognized by a decrease in intensity and a marked shift of the band at 3745 to 3727 cm^{-1} as well as the appearance of a new band at 3668 cm^{-1}. The latter band was produced by the interaction of the framework Al–OH with Mo species. The BET surface areas of Mo-dealuminated mordenite samples were higher than the corresponding Mo-free ones. The diffuse reflectance measurements suggested that Mo cations are predominantly present as an octahedrally coordinated Mo^{6+}, along with some tetrahedral Mo^{6+}. New spectral features as a consequence of dealumination events in the far-IR range were evaluated and discussed.

Key Words: **molybdenum oxide; Na–mordenite; dealumination; XRD; UV-DRS; N_2 adsorption; TGA; far-IR.**

INTRODUCTION

Mo/zeolite catalysts have been extensively employed in the petroleum industry for their valuable activities, e.g., hydrodesulfurization (HDS) and hydrodenitrogenation (HDN) reactions (1, 2) as well as epoxidation of cyclohexene, propylene, and toluene dealkyation (3–5). The methane aromatization reaction, which is carried out currently on the Mo/ZSM-5 catalyst, has attracted the attention of many researchers (6, 7). However, the conversion of methane to higher hydrocarbons on this catalyst was about 6–7% (8). Because of discrepancies among various research groups in identifying the active Mo species in the latter reaction, the accurate designation of these species was not achieved (6). Another area of disagreement concerned the distribution of Mo species in the zeolite. Nevertheless, no evidence regarding the exact location of Mo in zeolite is reported, although most researchers agreed that Mo ions were highly dispersed inside the zeolite lattice (6, 7, 9, 10).

Based on previous studies (6, 9, 10), it has been suggested that highly dispersed Mo species was obtained at 2–3 wt%, where bulk MoO_3 was confirmed at 6–10 wt%. In the latter range of Mo loadings, a marked decrease in the activity of the catalyst for the conversion of methane was recorded. This was regarded as a consequence of the decrease in the BET surface area, micropore volume, and zeolite crystallinity of ZSM-5 when loaded with Mo (9–11). These results were interpreted such that Mo can form multilayer oxides that extensively block the channel entrances (6). Thus, it is important to improve the above-noted physicochemical properties of Mo–zeolite catalysts.

In view of the importance of coordinatively unsaturated (cus) Al ions for supporting different metal cations such as Co, Mg, and Cr (12), mild steam dealumination of H-mordenite was lately carried out for the purpose of generating nonframework Al species, used for the stabilization of CO coordinating Au^+ (13). The zeolite dealumination by acid leaching exhibited a larger surface area, higher stability, and larger pores than that in parent zeolite (14, 15). Of particular interest, the dealuminated mordenite showed an excellent reactivity and stability in hydrocarbon reactions (16). Since mordenite can be dealuminated to a high degree without losing its crystallinity (17), it is an extremely useful substrate for studying the effect of residual aluminum on the dispersion of Mo ions. Another peculiar property is the acidity enhancement of dealuminated H-mordenite rather than the nondealuminated form. This could be associated with the Si/Al ratio (18) and the crystal structure (19).

Therefore, the objective of the current study is to obtain an insight into the effect of acid dealmination of the Na–mordenite zeolite on the dispersion of added Mo at a 12 wt% loading and to recognize the different Mo species. These catalysts were characterized by IR and UV-visible spectroscopies as well as XRD and TG techniques. Low temperature N_2 adsorption data were

[1] To whom correspondence should be addressed. E-mail: mohmok2000@yahoo.com.

0021-9797/02 $35.00

used to characterize the texture and pore structure of the dealuminated loaded Mo catalysts. Special attention was paid to the far-IR region (400–100 cm^{-1}) to bring about the effect of dealumination on the zeolite structure, the state and location of Mo ions that can hardly be refined in the mid-IR region (1300–400 cm^{-1}).

EXPERIMENTAL

Catalyst Preparation

The starting material sodium mordenite zeolite [E139 (NaM + 20% Al_2O_3) and HNO_3 as binder], designated as NaM, was acid-leached under various conditions of acid concentration, contact time, and temperature. The dealuminated zeolites were calcined at 773 K in air (0.5 K/min) over a period of 48 h prior to Mo incorporation. This step was carried out in order to avoid any dealumination sequences from the self-steaming process. The total aluminum contents of dealuminated Na–M, analyzed by classical chemical analysis, are listed in Table 1. The zeolite-loaded Mo were prepared by impregnation of nondealuminated and dealuminated mordenites with an aqueous solution of ammonium heptamolybdate, $(NH_4)_6Mo_7O_{24} \cdot 4H_2O$, at a concentration of 12 wt% Mo. These samples were dried at 393 K for 12 h and calcined at 773 K in air for 16 h. The samples were, respectively, referred to as NaMMo and Mo-dealuminated NaM (HM1–4 Mo).

Characterization Techniques

Infrared spectra were recorded using an FTIR Perkin-Elmer 1650 instrument with a spectral resolution of 2 cm^{-1}. Self-supporting wafers of similar thickness weighing approximately 20 mg were prepared using an applied pressure between 5 and 7 tons per square inch for up to 30 s. The spectra reported are the result of the coaddition of 300 interferograms encompassing a 15-min collection time.

UV-visible diffuse reflectance spectra were recorded using a Jasco Model V-570 unit UV-VIS spectrophotometer (Serial Number, C29635) equipped with a diffuse reflectance attachment. The Mo-loaded samples were studied in the form of 12-mm-diameter, 2-mm-thick pellets prepared as self-supporting wafers. The spectra were recorded under air-exposed conditions in the range 190–390 nm against the parent mordenite reference. In order to minimize the effect of rehydration of the calcined samples prior to spectral accumulation, the spectra were recorded at 5 min after removal of the pellets from the oven. The reference sample pellets were subjected to pretreatments similar to those of catalyst pellets.

X-ray powder diffraction patterns were obtained on a Philips diffractometer PW 1840 using Cu$K\alpha$ radiation at room temperature. Powder diffractograms of samples were recorded over a range of 2θ values from 5 to 60° under the conditions of 30 kV and 20 mA at a scanning rate of 5°/min. All the recorded XRD patterns can be processed with a computer system attached to the instrument.

Specific surface areas and average pore diameters of the different samples were obtained by the BET method at the liquid nitrogen temperature (77 K) using a conventional volumetric apparatus. Before carrying out the measurements, each sample was degassed under a reduced pressure of 10^{-5} Torr for 2 h at 573 K.

The zeolite water content after dealumination and Mo incorporation was determined by the TG technique over the temperature range from ambient to 873 K at a heating rate of 10 K/min under dry N_2 (40 cm^3 min^{-1}). The TG curves were automatically recorded on a Model 50 Shimadzu unit.

TABLE 1
Al Contents and Dealumination Procedures of the Mordenite Zeolite

Sample	Acid leaching procedure	Total Al (mmol g^{-1})	$(Si/Al)_f$[a]
NaM	E139 + 20% Al_2O_3 (parent)	3.36	5.73
HM1	NaM + 1 mol dm^{-3} HCl; 3 h; 298 K	2.8	5.6
HM2	NaM + 1 mol dm^{-3} HCl; 3 h; 373 (reflux)	2.6	4.4
HM3	NaM + 5 mol dm^{-3} HCl; 3 h; 298 K	2.5	4.26
HM4	NaM + 5 mol dm^{-3} HCl; 3 h; 373 K (reflux)	2.1	2.68
NaMMo	E139 + 20% Al_2O_3 + 12 wt% Mo		
HM1Mo	NaM + 1 mol dm^{-3} HCl; 3 h; 298 K + 12 wt% Mo		
HM2Mo	NaM + 1 mol dm^{-3} HCl; 3 h; 373 (reflux) + 12 wt%		
HM3Mo	NaM + 5 mol dm^{-3} HCl; 3 h; 298 K + 12 wt% Mo		
HM4Mo	NaM + 5 mol dm^{-3} HCl; 3 h; 373 K (reflux) + 12 wt%Mo		

[a] (Si/Al) is obtained from the equation: $(Si/Al)_f = (Si/Al)\,ch \cdot (Al_{total}/Al_{IV})$.

RESULTS AND DISCUSSION

IR Study of Dealuminated Mordenite Zeolites (1300–100 cm^{-1})

Figure 1 shows the vibrational spectra in the mid (1300–400 cm^{-1}) and far-IR (400–100 cm^{-1}) regions for different dealuminated Na–mordenite zeolites. The bands in the former region showed marked shifts to higher wavenumbers for symmetrical and asymmetrical TO_4 tetrahedra with dealumination, as compared to the original Na–mordenite (NaM) sample. The variations in wavenumbers due to dealumination are listed in Table 2. For example, the bands at 651 and 615 cm^{-1} were observed to vary with dealumination extent: the former band was shifted to 629 cm^{-1} with a decrease in intensity whereas the latter vanished. Similarly, the 719 cm^{-1} band almost vanished at the early dealumination stage (HM1). The band at 651 (629) cm^{-1} is due to isolated AlO_4, as interpreted by Van Geem *et al.* (21). The disappearance of the bands at 719 and 615 cm^{-1}, in the spectrum of HM1, confirms that they are associated with the surface aluminum species, which originally present in the

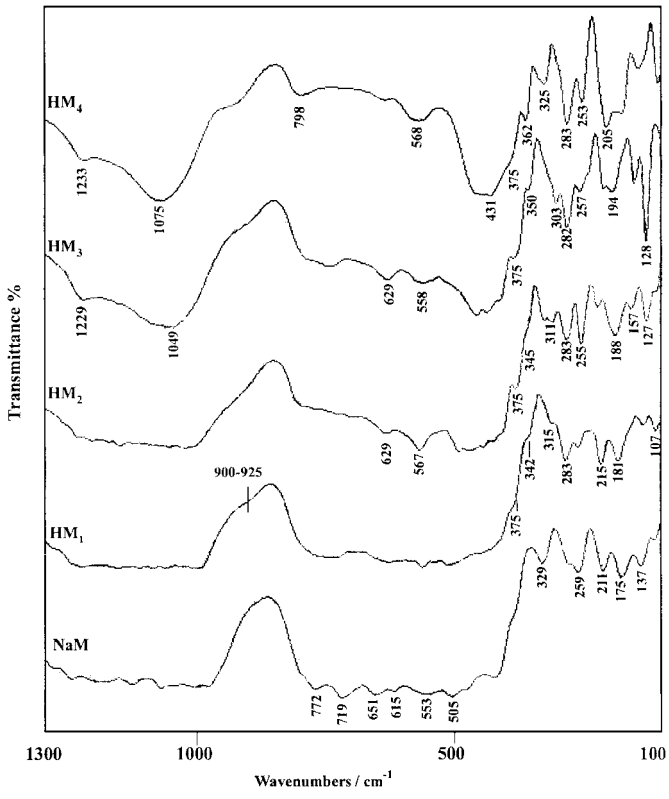

FIG. 1. Mid- and far-IR transmittance spectra of nondealuminated (NaM) and dealuminated HM1, HM2, HM3, and HM4 mordenite zeolites.

mother sample as an excess Al_2O_3 (20 wt%). The 772 cm^{-1} band showed an upward shift in wavenumbers to 798 cm^{-1}. This verifies that it is due to Al–O in alternating SiO_4 and AlO_4 tetrahedra. In addition, the broadband at 553 cm^{-1} is ascribed to T–O in 5-membered rings, as indicated by Lezcano *et al.* (22). Of particular importance, a shoulder at 900 cm^{-1} was depicted in the spectra of HM1–4. This shoulder was not apparent in the NaM spectrum. Accordingly, it is associated with TO_4 tetrahedra in [O–(Al, Si)–O] or in Si–O–Si involved structures. With higher dealumination this shoulder was more as evident by increasing its intensity and causing a marked shift to higher wavenumbers (925 cm^{-1}). The latter assignment is suppported by an analogous band at 955 cm^{-1} obtained by the acid dealumination of mordenite and ascribed to the Si–O–Si linkages (23). The 900 (925) cm^{-1} band was found to be synchronous with the asymmetric band occurring in the 1029–1075 cm^{-1} region that was used to measure the extent of Si atoms in the vacant sites left by leached Al (23).

In the FIR spectrum (400–100 cm^{-1}) of the NaM sample, bands at 329, 283 and 259, 211, 175, 137, and 107 cm^{-1} were clearly observed. Inspection of this region during the dealumination course revealed the following. First, the earlier disappearance of the 329 cm^{-1} band under mild acid leaching conditions (HM1) was indicative of a nonstructural aluminum species. A typical band was observed at 330 cm^{-1} in rare earth garnet aluminates such as $3R_2O_3 \cdot 5Al_2O_3$ and $3CaO \cdot Al_2O_3 \cdot 6H_2O$ and was attributed to isolated AlO_6 octahedra (24). Secondly, shoulders at 342 and 375 cm^{-1} were seen newly produced in the spectrum of HM1, whose positions and intensities were varied with dealumination level. The former shoulder turned to a distinct band in the spectrum of HM3 sample that diplayed a marked shift to 362 cm^{-1} with increasing dealumination (HM4). Thus, this band (342–362 cm^{-1}) is attributed to Al–O vibration belonging to alternating SiO_4 and AlO_4 tetrahedra. The behavior of this band was parallel to that in the 1029 (1075) cm^{-1} region, reflecting their correlation with structural band vibration, i.e., increased number of T vacancies as a function of extracted aluminum atoms. The shoulder at 375 cm^{-1} attained an appreciable increase in intensity with no change in position until HM3, and then vanished at HM4. This band can be due to AlO_4 tetrahedra either isolated and/or partially attached to the framework.

The bands at 259 and 283 cm^{-1}, which almost showed no change in their positions, were enhanced in intensity especially for samples dealuminated at the reflux temperature (HM2 and HM4). Hence, they are best attributed to T–O vibrations in 5-membered rings (25). The bands at 175 and 211 cm^{-1} in the spectrum of NaM sample showed marked enhancement in intensities and became ill-resolved with the dealumination level. Besides, the former band exhibited upward shifts to 194 cm^{-1}

TABLE 2
Mid- and Far-IR Frequencies of Dealuminated Mordenites and after Loadings with Mo

Sample	ν_{as}(T–O)		ν_s(T–O)			Vibration of double rings		δ(O–T–O)	Framework vibrations in the far-IR			
NaM		—		772	651	553	505	415	375	—	283	259
HM1		—	900	—	—	560	511	—	375	342	283	255
HM2	—	1029	900	—	629	567		—	375	345	283	255
HM3	1229	1049	900	746	629	558		465	375	350	282	257
HM4	1233	1075	900	798	629	568		431	375	362	282	253
NaMMo	1212	1067	900	800	630	577		450			276	
HM1Mo	1213	1062	900	802	632	563		458			280	
HM2Mo	1229	1081	900	804	635	565		461			280	
HM3Mo	1230	1044	925	800	633	554	565	472			280	
HM4Mo	1229	1054	925	798	633	570		450			286	

where the latter showed downward shifts to 205 cm^{-1}. It has been confirmed by Ozin and co-workers (26) that the only vibrations that can be ascribed to cation vibration modes occur below 200 cm^{-1}. This indicates that the bands in the 100–200 cm^{-1} region are diagnostic for the cation site and its population (27). By virtue, it is imperative to assign the 175 cm^{-1} band to Na^+ cations interacting inside mordenite channels. In addition, this band was in synchrony with the 211 (205) cm^{-1} band throughout the dealumination, confirming that they are originating from the same species. Therefore, these bands are ascribed to Na^+ cations influenced by acid dealumination, which was responsible for the ill-resolution of the bands (as in HM3 and HM4). Similar results were obtained for Na–Y zeolites (28).

The band at 137 cm^{-1} in the spectrum of NaM sample that showed a decrease in linewidth and a shift to lower wavenumbers with dealumination, HM1 (133), HM2 (127), and HM3 (127), is ascribed to Na^+ ions located in a definite channel. This is supported by vanishing of this band in the spectrum of HM4 sample. The sharpening of this band in the HM3 sample reflects the high population of Na^+ ions in mordenite channels where it totally vanished at the reflux temperature, as in the HM4 sample. A similar band at 145 cm^{-1} was obtained in a HNaY sample and attributed to the residual Na^+ ions at site I (29). The 107 cm^{-1} band that showed a marked decrease in intensity until HM3 is related to Na^+ ions. This was confirmed by an IR study of NaY zeolite that showed a band at 109 cm^{-1}, ascribed to Na^+ ions in site I^- (28). A band at 157 cm^{-1} that is primarily seen as a shoulder in the HM1 sample was distinctly observed when increasing the Si/Al ratio, reflecting the difficulty of reaching these Na^+ ions under mild acid leaching conditions. It can be seen that the band broadening resulting from the protonation effect (28), which has been obtained as a result of dealumination, ceases for Na^+ ions absorb at the lowest frequencies, i.e., 107, 137, and 157 cm^{-1}. However, their varied frequencies and intensities are dependent on the bonding of Na^+ ions to their neighboring lattice oxygens. By virtue, bands around 200, 150, 100, and 75 cm^{-1} were observed in Na–Faujasite zeolites at varying ratios of Si/Al (30).

IR Study of Mo-Encapsulated Dealuminated Mordenite

Figure 2 shows the IR spectra of nondealuminated and dealuminated Na–mordenite-loaded Mo samples. The spectrum of NaMMo (Fig. 2) showed significant spectral changes compared with that of NaM (Fig. 2) in the 1300–400 cm^{-1} region (Fig. 1). The existence of the 900 cm^{-1} band in the NaMMo spectrum on one hand and its shift to higher wavenumbers (925 cm^{-1}) with dealumination on the other hand suggest the formation of Mo–O–T bonds (30, 31). The 900 cm^{-1} band was not apparent in the NaM (Fig. 1) spectrum. It follows that an appreciable formation of the Mo–O–Si linkage is expected over the Mo–O–Al one with the decrease in the aluminum content. The vibrational frequencies of these linkages indicated an agreement with the former assignment based on a band in the 915–925 cm^{-1} region

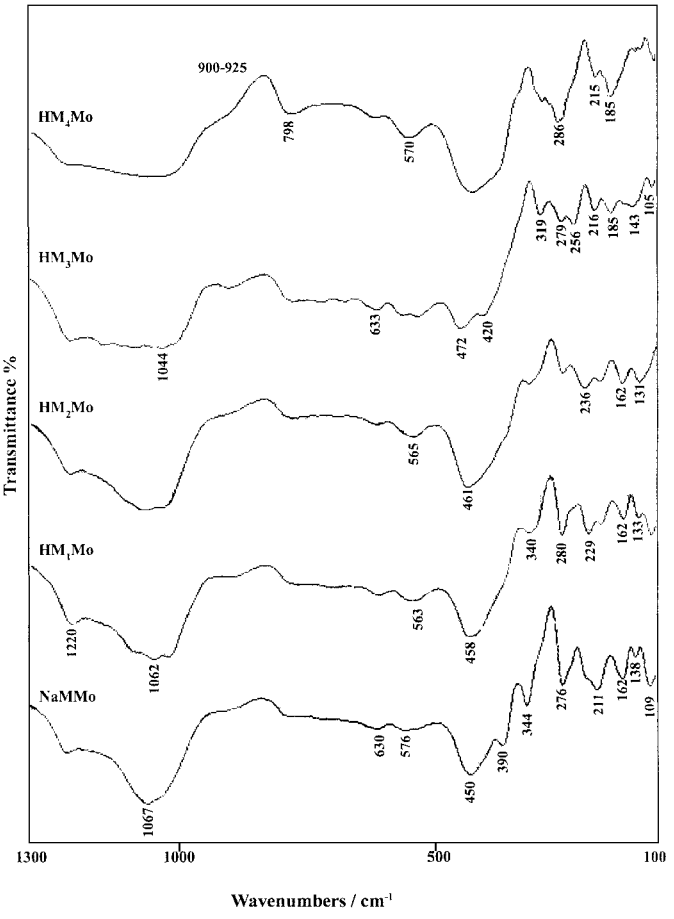

FIG. 2. Mid- and far-IR transmittance spectra of nondealuminated and dealuminated-mordenite-loaded Mo.

(32). However, the vibrational frequency ascribed to Mo–O–Al linkage was verified at 880 cm^{-1} (32).

On the other hand, the far-IR region (400–100 cm^{-1}) showed a number of bands that exhibited strong dependence on the cation mass. The spectrum of NaMMo shows new bands at 390 and 344 cm^{-1} when compared with the corresponding Mo-free NaM (Fig. 1). Thus, these bands can be due to molybdenum oxygen bond vibrations. However, the former band completely vanished after dealumination, confirming that it is related to Mo–O–Al vibration (33). The 344 cm^{-1} band showed a broadening and a decrease in intensity in favor of a new band at 319 cm^{-1}, at HM3Mo and HM4Mo. The vanishment of the former band in favor of the latter one was tentatively indicative of improvement in the Mo dispersion with dealumination, as a consequence of widening the average pore radius of zeolite, as will be presented later. In addition, depiction of the 319 cm^{-1} band at HM3Mo was indicative of the existence of other Mo–O moieties. The marked decrease of this band in the HM4Mo spectrum reflected as well the higher dispersion of Mo–O moieties with dealumination. A new band at 229 cm^{-1} demonstrated an intensity enhancement together with a shift to 236 cm^{-1}at HM2Mo; meanwhile it vanished at HM3Mo and HM4Mo. The bands occurring at 344, 319

and 229 (236) cm^{-1} that are related to single Mo–O bond vibrations are, respectively, attributed to δ(Mo–O) and δ(Mo–O–Mo) bridges (34). This result is in agreement with that observed by Banares *et al*. (35) during an IR study of dehydrated molybdenum oxide on Al_2O_3.

Interestingly, no bands for bulk MoO_3 were revealed. In agreement, the diffuse reflectance spectra (190–390 nm) of Mo-loaded dealuminated samples (Fig. 3) exhibited a band in the 312–321 nm region attributed to Mo^{6+} ions in an octahedral (polymeric) arrangement (36). A shoulder at 270 nm attributed to tetrahedral Mo^{6+} was also detected that was consistent with the work of Che *et al*. (37) on $MoCl_5$–silica. Figure 3 clearly indicates the absence of bands related to either tetrahedral coordinated Mo ions (230 nm) (35, 36) or bulk MoO_3 , which used to appear as a broadband near 330 nm (38).

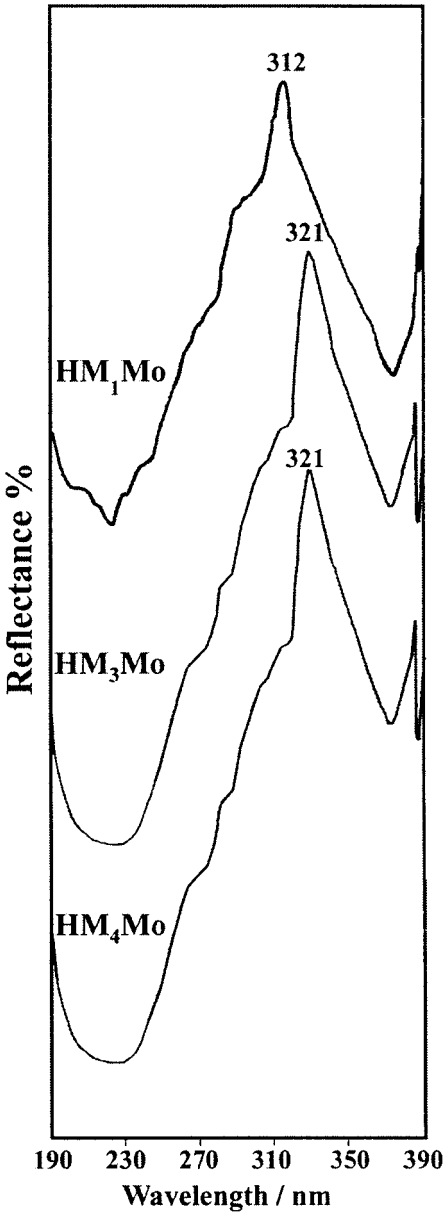

FIG. 3. Selected ultraviolet diffuse reflectance spectra of dealuminated mordenite-loaded Mo.

The vibrational mode at 276 (286) cm^{-1} in the NaMMo spectrum (Fig. 2), which is related to framework structure, was accompanied by a marked decrease in intensity during dealumination, except that in the HM4Mo spectrum which exhibited a band broadening. This might reveal the strong interaction between Mo species and the lattice framework. However, the broadening of the band is a consequence of the effect of reduced Mo occupancy as a result of increasing the Si/Al ratio, as observed for Hi Sil-sod (25).

The bands at 162, 138, and 109 cm^{-1} previously ascribed to Na^+ cations residing in different sites inside mordenite channels showed marked spectral changes following Mo incorporation (Fig. 2). The former band showed a decrease in intensity upon Mo addition at HM1Mo and HM2Mo. The 138 cm^{-1} band was shifted to lower wavenumbers with dealumination, i.e., 133 and 131 for HM1Mo and HM2Mo, respectively. The 138 (131) cm^{-1} band with that at 162 cm^{-1} overlaped at 143 cm^{-1} in the HM3Mo spectrum and disappeared at HM4Mo. This could be attributed to the expected weaker electrostatic interaction of Mo ions with the oxygen atoms in the framework rather than with Na^+ ions. The observed decrease in intensity of this band (143 cm^{-1}) as well as the lower shift in wavenumbers indicated the presence of residual Na^+ nearby Mo^{6+} in the same site. This can be confirmed from either band broadening in the spectrum of HM2Mo or splitting in the spectrum of HM4Mo. Small shifts were noted for the 109 cm^{-1} band to 105 cm^{-1} at the higher extent of dealumination (HM4Mo) to confirm the lower sensitivity of this site to cation exchange. Thus, these small shifts could be a consequence of population and angular effects (29).

IR Study of Surface Hydroxyl Groups

Figure 4 illustrates the spectral changes associated with the hydroxyl groups in the (4000–3250 cm^{-1}) region at increasing dealumination levels. Before dealumination, the NaM zeolite showed a band at 3628 cm^{-1}, characteristic of acidic OH groups, and a band at 3443 cm^{-1}, characteristic of hydrogen bonding hydroxyl groups. The latter groups were not too near each other but are still able to form weak hydrogen bonding (39). It should be noted that the high frequency hydroxyl of terminal silanol groups did not exist in the NaM spectrum due to the presence of extraframework aluminum, as Al_2O_3 on the outer surface. Besides, other hydroxyl groups emerged at 3291 cm^{-1} that likely originated from water-attached OH groups (39) and/or underwent perturbation through attaching to neighboring oxygen atoms of the framework (hydrogen bonding) (40). The latter assignment stemmed from the band shape that appeared strong.

Upon dealumination (spectra HM1–HM3), the acidic OH groups at 3628 cm^{-1} showed a decrease in intensity with a parallel increase in intensity in the terminal Si–OH band at 3742 cm^{-1}, as in the HM2 spectrum. This observation strongly emphasized the assignment of the 3628 cm^{-1} band to acidic OH

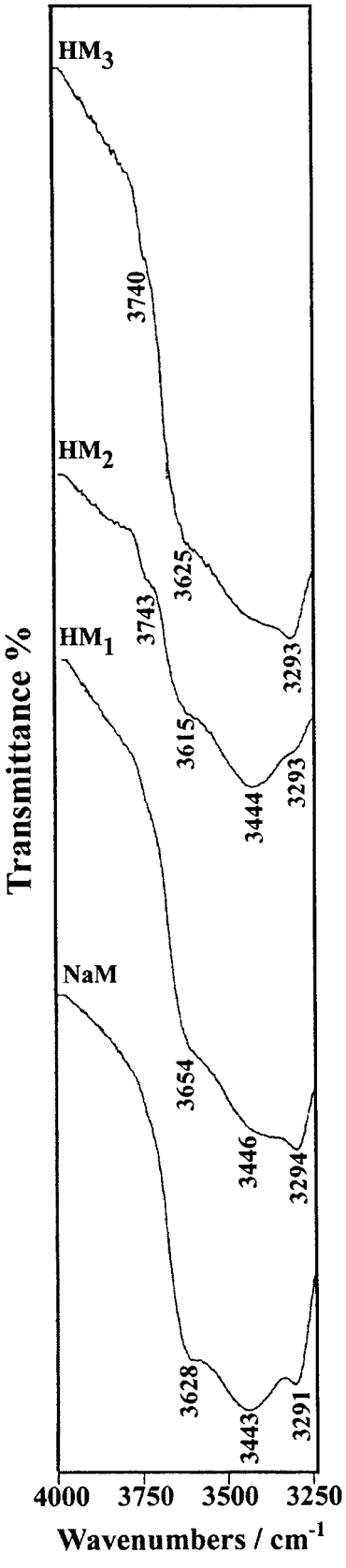

FIG. 4. The OH stretching frequencies of parent NaM and after acid leaching: (a) NaM, (b) HM1, (c) HM2, (d) HM3.

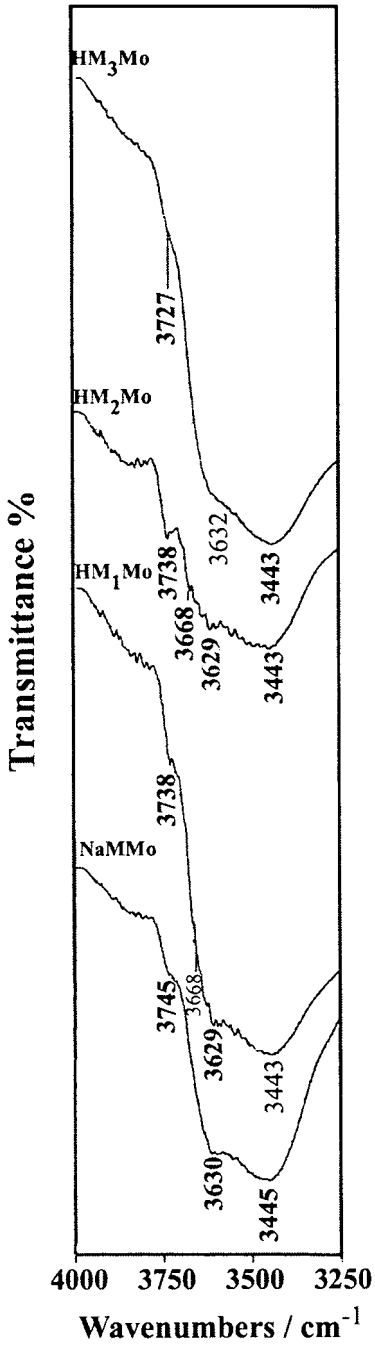

FIG. 5. The OH stretching frequencies of nondealuminated and dealuminated mordenite-loaded Mo: (a) NaMMo, (b) HM1Mo, (c) HM2Mo, (d) HM3Mo.

groups of Brønsted type, as proposed by Topsoe *et al*. (41). It can be seen that the nature of the 3743 cm^{-1} band is also correlated to the perturbations of the bands at 3446 and 3293 cm^{-1}. More interestingly, these bands showed different intensity changes during the dealumination, confirming that they are of different types. The hump of silanol groups at 3740 cm^{-1} is due to nonacidic hydroxyls that resided in sites vacated by aluminum atoms.

Figure 5 shows the IR spectra of nondealuminated and dealuminated NaM-loaded Mo in the 4000–3250 cm^{-1} region. The NaMMo spectrum is characterized by a shoulder at 3745 cm^{-1} that did not exist in the NaM sample (Fig. 4), along with the bands at 3630 and 3445 cm^{-1}. The Mo addition causes the disappearance of the 3291 cm^{-1} band, suggesting the interaction of the Mo species with the OH groups bonding the lattice oxygen. Comparison of the IR results in Figs. 4 and 5 revealed the following. (i) A shoulder at 3668 cm^{-1} in the IR spectra of HM1Mo and HM2Mo, that was not seen in the NaMMo spectrum, is ascribed to OH groups attached to nonstructural aluminum (42). However, this band was not produced in spectra of Fig. 4, suggesting the intricacy of assigning this band to OH groups attached to nonstructural Al. Therefore, it is likely that this band is attributed to OH vibrations derived from the interaction with Mo species. This is plausibly due to the shift of this band to relatively higher frequencies, i.e., 3668 cm^{-1}, than those reported for OH attached nonstructural Al, i.e., 3650 (3660) cm^{-1}. The weak intensity of the band at 3668 cm^{-1} could also ascertain the latter assignment. On the other hand, the disappearance of this band in the HM3Mo sample was indicative of the high dispersion of Mo inside the internal zeolite surface at high acid dealumination. An IR study on the surface aluminum sites of MCM-41 in the OH stretching region indicates a band at 3688 cm^{-1} assigned to molecular water (43). This is unlikely because of the disappearance of the band at 3291 cm^{-1}.

The band at 3745 cm^{-1} showed a decrease and a shift to lower wavenumbers (3727 cm^{-1}), indicating that a strong interaction between Mo and terminal silanol groups has been taken place. The Si–OH band shift from 3740 to 3727 cm^{-1} upon Mo addition was markedly higher than the corresponding shift of the SiOHAl band from 3632 to 3629 cm^{-1}, indicating that the interaction of Mo with the former sites was much stronger and, hence, the acid strength is far improved (44). This improvement is correlated with the ionic character of H atoms since the electronegativity of the OH bond attached to Si-rich zeolite, as a result of dealumination, is of higher electronegativity compared with Al atoms.

Surface Properties, Crystallinity, and Water Content of the Samples

The physicochemical characteristics of the studied samples are listed in Table 3. It can be seen that the unit cell dimensions are reduced during dealumination, suggesting that some aluminum atoms are expelled from the crystal lattice. Particularly, the lattice dimensions of *a* and *c* showed a fast contraction with dealumination as compared with that of *b*. The overall effect is the marked decrease in unit cell volume. These changes were accompanied by a noticeable increase in the relative crystallinities of the dealuminated samples except HM4 which showed the lowest crystallinity. On the other hand, a marked increase in the unit cell volume for HM1Mo and HM3Mo samples compared with the corresponding Mo free ones was obtained, indicating the well dispersed Mo ions inside the former samples. This result was also confirmed from the evident decrease in crystallinities of Mo-dealuminated samples compared with those of Mo-free dealuminated ones. Detailed analysis of the XRD results did not show evidence of the MoO_3 phase.

The effect of dealumination on the texture of NaM was apparent from the marked increase in the external surface. This effect can be ascribed, as already evidenced (45), to the formation of mesopores during dealumination that may be accompanied by the collapse of some micropore blocking. The surface areas of Mo dealuminated samples were higher than those of Mo-free ones, indicating that some of the deposited Mo species in

TABLE 3
Thermal Data, Cell Constants, Crystallinities, and Textural Properties of the Studied Samples

Catalyst	BET (m^2/g)	$S^{t a}$ (Ext m^2/g)	Vt[b] (cm^3 g^{-1})	TGA[c] Wt% H_2O	Crystallinity[d] (%)	Cell constants (Å)			
						a	*b*	*c*	*V* $(A^\circ)^3$
NaM	408	72	0.182	13.9	100	18.028	20.191	7.464	2715.2
HM1	401	78	0.178	11.3	110	18.01	20.100	7.464	2700.5
HM2	390	80	0.170	12.1	107	18.00	20.100	7.464	2700.5
HM3	389	98	0.161	12.5	120	17.95	20.09	7.450	2686.6
HM4	380	101	0.153	12.2	90	17.21	20.10	7.17	2480.3
NaMMo	430	69	0.178	11.5	98	18.053	20.224	7.431	2711.7
HM1Mo	423	73	0.168	14.4	100	17.984	20.495	7.420	2733.6
HM2Mo	418	77	0.160	15.4	94	17.985	19.862	7.338	2622.4
HM3Mo	416	85	0.153	14.2	107	18.279	20.304	7.516	2790.6
HM4Mo	410	93	0.140	15.8	83	16.953	18.344	6.840	2126.3

[a] External surface.

[b] Micropore volume determined by the *t* plot method.

[c] TGA loss in weight in the 293–873 K region.

[d] The crystallinity was obtained from the sum of the intesities of the 111, 130, 241, 002, 511, and 530 diffraction lines. The original Na–mordenite was taken as reference of 100% crystallinity. *V* is the unit cell volume $a * b * c$.

mesopores are responsible for the marked increase in S_{BET} probably due to the formation of their own texture. The micropores volume (V^t) values of the Mo-loaded dealuminated mordenite, which were determined using the approach of Remy and Poncelet (45), were lower than either those of Mo-free dealuminated samples or that of the parent NaM. This may possibly be due to the presence of MoO_3 particles in mordenite channels.

Thermogravimetric analysis (Table 3) indicates that the weight loss of the dealuminated samples in the 293–873 K range, which is associated with the removal of water, decreases as the total aluminum content decreases. On the other hand, the Mo-loaded dealuminated samples showed a higher weight loss than those of Mo-free dealuminated ones, reflecting the adsorption effect caused by Mo ions. In a DSC study (46), two desorption maxima were displayed when a cation-exchanged Na^+ in HM took place. The low temperature peak with a maximum around 383 K represents bulk water; i.e., water fills the pores but has no strong interaction with the framework structure. The desorbed amounts of water between 393 and 873 K are often small but the energy necessary per molecule is larger than that at low temperatures.

Given that the structure of Mo within the dealuminated samples is an octahedral, as emphasized from both IR and UV analyses, one must correlate that part of the observed decrease in crystallinity of Mo-containing samples is to the high water contents associated with these samples. This explaines the shift of some polymolybdate modes such as δ(Mo–O) into lower wavenumbers (344–319 cm^{-1}), as a function of dealumination (hydrophilic part in zeolite), as well as the presence of the δ(Mo–O–Mo) mode at its lower limit of frequency, at 229 cm^{-1} (47).

CONCLUSION

This paper demonstrated the sensitivity of far-Infrared for probing the cation modes and their locations in mordenite channels prior to and after delumination. In light of this, the following is deduced.

(1) Bands that are shifted and showed variations in the far-IR and attributed to lattice vibrations were 342–362, 375, and (259, 283) cm^{-1}. They were attributed to Al–O belonging to alternating SiO_4 and AlO_4 tetrahedra, isolated AlO_4 tetrahedra and/or partially attached to the framework, and T–O vibrations in 5-membered rings, respectively. Four different far-IR Na^+ modes, in dealuminated NaM samples, were detected at 157, 145, 137, and 107 cm^{-1}, which were considered as evidence for different interactions of Na^+ with zeolitic oxygen lattice. Undoubtedly, the identification of surface Mo oxide species in the 1100–400 cm^{-1} region is not an easy task because of the supperimposition of framework bands. However, following Mo species in the far-IR indicates two bands at 344 and 319 cm^{-1} attributed to δ(Mo–O) of polymolybdate species in addition to a band at 229 (236) cm^{-1} due to δ(Mo–O–Mo). The UV-diffuse reflectance spectra showed that these species are incorporated octahedrally into the dealuminated mordenites with no probability of forming an MoO_3 phase, as has also been confirmed by XRD and IR results. These results revealed the dispersion of MoO_3 species.

(2) As a consequence of acid dealumination, Mo-dealuminated mordenites showed higher surface areas than those of Mo-free ones. The affinity of Mo encapsulated in dealuminated mordenites to water adsorption reflected varying interactions of water with Mo. This interaction showed no effect on the Mo coordination inside the zeolite framework.

REFERENCES

1. Prinetto, F., Cerrato, G., Chiotti, G., Chiorino, A., Campa, M. C., Gazzoli, D., and Indovina, V., *J. Phys. Chem.* **99,** 5558 (1995).
2. Fierro, J. L. G., Conesa, J. C., and Agudo, L., *J. Catal.* **108,** 334 (1987).
3. Sohn, J. R., and Lunsford, J. H., *J. Catal.* **64,** 173 (1980).
4. Mizuno, K., and Lunsford, J. H., *J. Mol. Catal.* **27**(1-2), 1 (1984).
5. Yuan, C., Yao, J.-L., and Huang, M., *J. Shiyou Huagong.* **21,** 724 (1992).
6. Wang, D., Lunsford, J. H., and Rosynek, M. P., *J. Catal.* **169,** 347 (1997).
7. Wang, L., Tao, L., Xie, M., Xu, G., Huang, J., and Xu, Y., *Catal. Lett.* **21,** 35 (1993).
8. Solymosi, F., Erdohelyi, A., and Szoke, A., *Catal. Lett.* **32,** 43 (1995).
9. Chen, L., Lin, L., Xu, Z., Li, X., and Zhang, T., *J. Catal.* **157,** 190 (1995).
10. Xu, Y., Liu, S., Wang, L., Xie, M., and Guo, X., *Catal. Lett.* **30,** 135 (1995).
11. Xu, Y., Liu, W., Wong, S., Wang, L., and Guo, X., *Catal. Lett.* **40,** 207 (1996).
12. Karge, H. G., and Derouane, E. G. (Eds.), "Zeolites Microporous Solids: Synthesis, Structure and Reactivity" Kluweer, Dordrecht, 1992.
13. Mohamed, M. M., Salama, T. M., Ohnishi, R., and Ichikawa, M., *Langmuir* **17,** 5678 (2001).
14. Campbell, S. M., Bibby, D. M., Goddington, J. M., and Howe, R. F., *J. Catal.* **161,** 350 (1996).
15. Alexander, S. M., Goddington, J. M., and Howe, R. F., *Zeolites* **11,** 368 (1991).
16. Wang, I., Chen, T. J., Chao, K. J., and Tsai, T. C., *J. Catal.* **60,** 140 (1979).
17. Eberly, P. E., and Kimberlin, C. N., *Ind. Eng. Chem. Prod. Res. Dev.* **9,** 335 (1970).
18. Jacobs, P. A., *Catal. Rev.-Sci. Eng.* **24,** 415 (1982).
19. Senchenya, I. N., Kazansky, V. B., and Bernas, S., *J. Phys. Chem.* **90,** 4857 (1986).
20. Boudart, P., Nagy, J. B., Debras, G., Gabelica, Z., and Jacobs, P. A., *J. Phys. Chem.* **90,** 5183 (1986).
21. Van Geem, P. C., Scholle, K. F. M., Van der Velden, G. P. M., and Veeman, W. S., *J. Phys. Chem.* **92,** 1585 (1988).
22. Lezcano, M., Ribotta, A., Miro, E., Lombardo, E., Petunchi, J., Moreaux, C., and Dereppe, J. M., *J. Catal.* **168,** 511 (1997).
23. Van Niekerk, M. J., Fletcher, J. C. Q., and Oconnor, T., *J. Catal.* **138,** 150 (1992).
24. Tarte, P., *Spectrochim Acta* **23A,** 2127 (1967).
25. Baker, M. D., Ozin, G. A., and Godber, J., *J. Am. Chem. Soc.* **107,** 3033 (1985).
26. Godber, J., and Ozin, G. A., *J. Phys. Chem.* **92,** 2841 (1988).
27. Mortier, W. J., "Compilation of Extraframework Sites in Zeolites." Butterworth, Washington, DC, 1982.
28. Jacobs, W. P. J. H., Van Wolput, J. H. M. C., and Van Santen, R. A., *Zeolites* **13,** 171 (1993).
29. Ozin, G. A., Baker, M. D., Godber, J., and Gil, C. J., *J. Phys. Chem.* **93,** 2899 (1989).
30. Agudo, A. L., Benitez, A., Fierro, J. L. G., Palacios, J. M., Neira, J., and Cid, R., *J. Chem. Soc., Faraday Trans.* **88,** 385 (1992).
31. Mohamed, M. M., and El Shafei, G. M. S., *Spectrochim. Acta* A **51,** 1525 (1995).
32. Jeziorowski, H., and Knozinger, H., *J. Phys. Chem.* **83,** 1166 (1979).

33. Zingg, D. S., Makovsky, L. E., Tischer, R. E., Brown, F. R., and Herclues, D. M., *J. Phys. Chem.* **84,** 2898 (1980).
34. Okamoto, Y., and Imanaka, T., *J. Phys. Chem.* **92,** 7102 (1988).
35. Banares, A., Hu, H., and Waches I. E., *J. Catal.* **150,** 407 (1994).
36. Fournier, J., Louis, C., Che, M., Chaquin, P., and Masure, D., *J. Catal.* **119,** 400 (1989).
37. Che, M., Figueras, F., Forissier, M., Mcateer, J., Perrin, M., Portefaix, J. L., and Praliaud, H., "Proceedings of the Sixth International Congress on Catalysis, London, 1976 (G. C. Bond, P. B. Wells, and F. C. Tompkins, Eds.), p. 261. Chem. Soc., London, 1976.
38. Wang, L., and Hall, W. L., *J. Catal.* **77,** 232 (1982).
39. El Shafei, G. M. S., and Mohamed, M. M., *J. Colloid Interface Sci.* **175,** 518 (1995).
40. Zholobenko, V. L., Kustov, L. M., Borovkov, V. Yu., and Kazansky, V. B., *Zeolites* **8,** 175 (1988).
41. Topsoe, N., Pedersen, K., and Derouane, E. G., *J. Catal.* **70,** 41 (1981).
42. Viale, S., Garrone, E., Di Renzo, F., Chiche, B., and Fajula, F., *Stud. Surf. Sci. Catal.* **105,** 533 (1997).
43. Wang, D., Lunsford, J. H., and Rosynek, M. P., *J. Catal.* **169,** 347 (1997).
44. Arean, C. O., Platero, E. E., Mentruit, M. P., Delgado, M. R., Xamera, F. X. L., Garcia-Raso, A., and Morterra, C., *Microporous Mesoporous Mater.* **34,** 55 (2000).
45. Remy, M. D., and Poncelet, G., *J. Phys. Chem.* **99,** 773 (1995).
46. Mohamed, M. M., *Thermochim. Acta* **230,** 167 (1993).
47. Stencel, J. M., Makovsky, L. E., Sarkus, T. A., De Vries, J., Thomas, R., and Moulijn, N., *J. Catal.* **90,** 314 (1984).